Open Access

Recent Progress in Science and Engineering

LIDSEN Publishing Inc.

Original Research

A Fuel Cell Control System for Performance Improvement under Variable Atmospheric Pressure Conditions

Carlos Armenta-Déu *

Dpt. Of Matter Structure, Thermal Physics and Electronics, Faculty of Physics, Complutense University of Madrid, 28040 Madrid, Spain; E-Mail: cardeu@fis.ucm.es

* **Correspondence:** Carlos Armenta-Déu; E-Mail: cardeu@fis.ucm.es

Academic Editor: Orlando Corigliano

Recent Prog Sci Eng
2025, volume 1, issue 1
doi:10.21926/rpse.2501001

Received: September 20, 2024
Accepted: January 09, 2025
Published: January 20, 2025

Abstract

This work focuses on designing a control unit for improving Proton Exchange Membrane Fuel Cell (PEMFC) performance powering electric vehicles when operating in variable atmospheric pressure conditions, a current situation in mountainous countries with sudden changes in road altitude. The paper studies and analyzes the PEM fuel cell behavior working with hydrogen supply from a pressurized tank and oxygen input from atmospheric air supply in journeys with continuous variation of road level due to the orography. The work proposes a control unit that regulates hydrogen and oxygen partial pressure to match each other, assuring correct fuel cell operation and improving performance. A simulation for a fuel cell powering a standard electric vehicle shows that fuel cell performance improves by 8.5%, enlarging the driving range by 7.8% and prolonging the fuel cell lifespan. The control unit is adaptive to all-electric vehicles powered by a PEM fuel cell. Although the simulation test runs for altitudes between sea level and 2000 m, it is valid for any altitude variation from sea level to 6000 meters, representing the practical totality of world roads.

Keywords

Proton exchange membrane fuel cell; electric vehicle; road altitude variation; control system; performance improvement; hydrogen wasting; driving range

1. Introduction

In a world engaged by the energy transition from fossil fuels to renewable sources due to the continuous growth of carbon emissions, the transportation sector plays a critical role in the planet's decarbonization since it represents one-third of GHG global emissions [1-4]. Worried about the effects of climatic change on human lives, politicians urge scientists and technicians to develop new power engines more respectful of the environment, either developing more efficient internal combustion engines with lower GHG emissions levels or powering vehicles with electricity generated by renewable sources; among this last option, two technologies apply, electric batteries and hydrogen [5, 6].

Electric batteries use lithium as the principal component for electricity generation, becoming the most popular system to power electric vehicles today [7, 8]. Nevertheless, the planet's lithium reserves are limited, and the continuous demand for this element represents a challenge that may derive from the lack of primary matter for electric batteries, causing the blockage of battery production and battery-powered electric vehicle development [9-13].

An alternative to lithium batteries is hydrogen [14, 15], an abundant element on our planet [16, 17]; hydrogen, however, is not an energy in pure form but an energy vector [18], meaning that its production requires previous transformation for the primary matter where the hydrogen is. Despite this, many experts conclude that hydrogen is the power source for the future in the transportation sector [19-21].

Electric vehicles powered by fuel cells currently use Proton Exchange Membrane (PEM) units because of their fast response, which is critical for vehicle operation [22]. The PEM fuel cell (PEMFC) operates based on hydrogen and oxygen supply; the oxygen may come from a reservoir tank (pure oxygen) or simply from the atmospheric air, which contains approximately 21% oxygen [23, 24]. Since the air does not contain hydrogen, this element must be produced and stored for later use in the PEMFC.

Hydrogen generation derives from two processes: hydrocarbon reforming and electrolysis. The first process requires high temperatures and produces carbon emissions, while the second only needs distilled water and electric current. From the environmental protection point of view, electrolysis is more suitable; however, it requires a water distillation process, reducing the process's applicability. Either way, hydrogen must be produced and stored for fuel cell operation [25-29].

The electro-oxidation process in the fuel cell requires a perfect balance between hydrogen and oxygen supply to operate at optimum performance; any variation of chemical reaction conditions results in a performance loss and lowered output power. Under these conditions, the electric vehicle powered by the fuel cell reduces its driving range while the PEMFC lifespan shortens.

Environmental conditions like atmospheric pressure influence the chemical reaction in the fuel cell, altering the stoichiometry, reducing the power generation, and lowering the efficiency. This paper develops a control unit to make the fuel cell operate at optimum conditions if the environmental conditions change, regulating partial pressures of hydrogen and oxygen to maintain the electro-oxidation chemical reaction unaltered.

The principal novelty of the proposed method is the fuel cell pressure supply management to optimize the performance. In current practice, the fuel cell operates under the basis of a regulated

oxygen flow supply with no pressure regulation, which is suitable for constant or low atmospheric pressure variation. This paper proposed a new method of fuel cell operation that is ideal for all atmospheric conditions. Despite the methodology used for Proton Exchange Membrane Fuel Cells (PEMFCs), it applies to any fuel cell working with atmospheric oxygen supply like Direct Methanol (DMFC), Alkaline (AFC), and Solid Oxide (SOFC).

The paper includes the following sections: Fundamentals, which deals with the theoretical principles supporting the article development; Engineering Design and Operation, which shows the components and elements of the system layout and describes the operational mode of the project; Power and Driving Range that evaluates the vehicle performance related to the power consumption; Simulation, which assesses the system performance, Data Analysis, corresponding to the analysis of simulation results, Driving Range, which evaluates the vehicle autonomy, and Fuel Cell Applications that includes alternatives to the selected fuel cell type. The final section corresponds to the Conclusions that summarize the principal aspects of the article.

2. Fundamentals

A fuel cell is a thermodynamic system in which hydrogen and oxygen flow to the anode and cathode (Figure 1) [30].

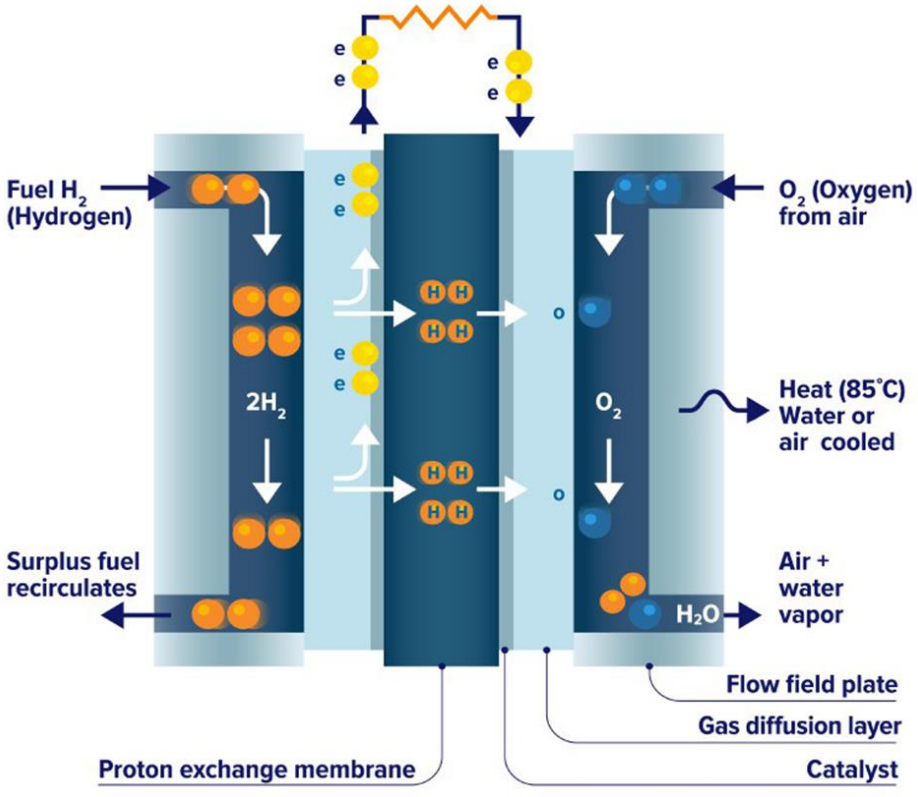

Figure 1 Schematic view of a Proton Exchange Membrane Fuel Cell (PEMFC) [30].

The electro-oxidation process at the fuel cell corresponds to the chemical reaction:

$$H_2 + \frac{1}{2}O_2 \rightarrow H_2O \quad (1)$$

In case the oxygen proceeds from the atmosphere, the electro-oxidation reaction of equation 1 transforms into [31]:

$$H_2 + \lambda^o(O_2 + 3.76N_2) \rightarrow H_2O + (\lambda^o - 0.5)O_2 + 3.76\lambda^o N_2 \quad (2)$$

λ^o is the stoichiometry coefficient for standard conditions equal to or greater than 0.5.

The coefficient 3.76 for the nitrogen molecule derives from the atmospheric air composition, where the nitrogen to oxygen ratio is 3.76, considering 79% of the air is nitrogen and 21% is oxygen.

Expressing the energy generated by a fuel cell in electric terms:

$$P_t = IV = \frac{\xi}{t} \quad (3)$$

P_t is the power generation, *I* and *V* are the fuel cell output current and voltage, and *t* is the operating time.

We can express the output current in terms of hydrogen mass react, F_{H_2} (mol/s), as:

$$I = F_{H_2} nF \quad (4)$$

n is the number of exchanged electrons and *F* is the Faraday number.

For the electro-oxidation process:

$$P_t = \frac{2ne^-}{t}V = \frac{\xi}{t} \rightarrow \xi = 2ne^-V \quad (5)$$

e^- is the electron charge.

The alternative expression for the output power and energy, using the output current equation (4) is:

$$P_t = F_{H_2} nFV = \frac{\xi}{t} \rightarrow \xi = F_{H_2} nFVt \quad (6)$$

Expressing equation 1 in terms of mass flow, it results:

$$\dot{n}_{H_2} + \frac{1}{2}\dot{n}_{O_2} \rightarrow \dot{n}_{H_2O} \quad (7)$$

$\dot{n}$ represents the molecular flow.

Defining the molecular flow in terms of mass flow, $\dot{m}$, yields:

$$\dot{n}_\iota = \frac{\dot{m}_\iota}{M_i} \quad (8)$$

M is the molecular mass.

Now, expressing the mass flow as a function of volumetric flow:

$$\dot{n}_i = \frac{\rho_i \dot{V}_i}{M_i} \quad (9)$$

And because the gas density depends on pressure, equation 9 transforms into:

$$\dot{n}_i = \frac{\rho_i^o p_i \dot{V}_i}{M_i} \tag{10}$$

Super-index *o* accounts for atmospheric pressure, and *p* is the partial pressure of component *i*.

Therefore, equation 7 converts into:

$$\frac{\rho_{H_2}^o p_{H_2} \dot{V}_{H_2}}{M_{H_2}} + \frac{1}{2}\frac{\rho_{O_2}^o p_{O_2} \dot{V}_{O_2}}{M_{O_2}} \rightarrow \frac{\rho_{H_2O(v)}^o p_{H_2O(v)} \dot{V}_{H_2O(v)}}{M_{H_2O}} \tag{11}$$

Since molecular mass and density at atmospheric conditions are constant, equation 11 transforms into:

$$\frac{p_{H_2} \dot{V}_{H_2}}{\gamma_{H_2}^o} + \frac{1}{2}\frac{p_{O_2} \dot{V}_{O_2}}{\gamma_{O_2}^o} \rightarrow \frac{p_{H_2O(v)} \dot{V}_{H_2O(v)}}{\gamma_{H_2O}^o} \tag{12}$$

γ^o represents the specific molecular volume at atmospheric pressure, which is constant.

To maintain the electro-oxidation reaction stoichiometry, the denominator of the reagents should remain constant; therefore, the volumetric flow is inversely proportional to the gas pressure. Relating partial and atmospheric pressure:

$$p_i = x_i p_{atm} \tag{13}$$

Xi is the gas fraction in the air.

Now, replacing in equation 12:

$$\frac{x_{H_2} p_{H_2} \dot{V}_{H_2}}{\gamma_{H_2}^o} + \frac{1}{2}\frac{x_{O_2} \dot{V}_{O_2} p_{atm}}{\gamma_{O_2}^o} \rightarrow \frac{x_{H_2O(v)} p_{H_2O(v)} \dot{V}_{H_2O(v)}}{\gamma_{H_2O}^o} \tag{14}$$

Considering that the oxygen fraction in the air remains constant, and standardizing terms in equation 14:

$$\beta_{H_2}^o p_{H_2} \dot{V}_{H_2} + \frac{1}{2}\beta_{O_2}^o \dot{V}_{O_2} p_{atm} \rightarrow \beta_{H_2O}^o p_{H_2O(v)} \dot{V}_{H_2O(v)} \tag{15}$$

With:

$$\beta_i^o = x_i / \gamma_i^o \tag{16}$$

Because the stoichiometry changes with gas partial pressure, equation 2 converts into:

$$H_2 + \lambda_r(O_2 + 3.76N_2) \rightarrow H_2O + (\lambda_r - 0.5)O_2 + 3.76\lambda_r N_2 \tag{17}$$

λ_r is the stoichiometry coefficient for non-atmospheric conditions, defined as:

$$\lambda_r = \lambda^o \frac{p}{p_{atm}} \tag{18}$$

Molecular hydrogen oxidizes at the anode releasing two electrons:

$$H_2 \rightarrow 2H^+ + 2e^- \tag{19}$$

At the cathode, the oxygen reduces according to:

$$\frac{1}{2}O_2 + 2e^- \rightarrow O^= \tag{20}$$

The oxidation-reduction process produces water vapor:

$$\left.\begin{matrix} H_2 \rightarrow 2H^+ + 2e^- \\ \frac{1}{2}O_2 \rightarrow O^= - 2e^- \end{matrix}\right\} H_2 + \frac{1}{2}O_2 \rightarrow (2H^+ + 2e^-) + (O^= - 2e^-) \rightarrow H_2O(v) \tag{21}$$

For specific hydrogen flow, $\dot{V}_{H_2}$, the generated current is:

$$I = 3.2 * 10^{-19} \frac{\rho^o_{H_2} p_{H_2} \dot{V}_{H_2}}{M_{H_2}} \tag{22}$$

The fuel cell output power is, therefore:

$$P_{FC} = 3.2 * 10^{-19} N \frac{\rho^o_{H_2} P_{H_2} \dot{V}_{H_2}}{M_{H_2}} V_{cell} \tag{23}$$

Since the oxidation-reduction reaction should be balanced, the output power as a function of the oxygen partial pressure can be expressed as:

$$P_{FC} = 1.6 * 10^{-19} N \frac{\rho^o_{O_2} p_{O_2} \dot{V}_{O_2}}{M_{O_2}} V_{cell} \tag{24}$$

V_{cell} is the output voltage of a single cell, and N is the stack cell number.

If partial hydrogen or oxygen pressure changes, the mole number arriving at the anode and cathode also changes, according to equation 10; therefore, the balance at equation 23 alters, and a hydrogen or oxygen mass flow fraction does not react, producing a hydrogen or oxygen surplus. In such a case, the electronic exchange modifies, so the generated current does.

In an unbalanced oxidation-reduction process, with constant hydrogen pressure flow, two situations arise: a partial oxygen pressure excess or a defect. The first situation does not produce fuel cell performance changes since the oxygen surplus is released to the atmosphere, flowing with the air stream; in the second case, a fraction of the molecular hydrogen flow cannot react, and the generated current lowers.

Applying the equation 24 to a reduced oxygen partial pressure:

$$F_P = \frac{P_{FC}}{P^o_{FC}} = \frac{p_{O_2}}{p^o_{O_2}} \tag{25}$$

F_P is the power factor. Super-index *o* accounts for the standard balance oxidation-reduction process.

The reader can notice that the output power reduction depends linearly on oxygen partial pressure lowering (see equation 25).

We can compensate for the power loss by reducing the hydrogen flow pressure to match the oxygen partial pressure so the oxidation-reduction process continues to be balanced; this avoids a hydrogen flow surplus and maintains the electronic exchange balance and the fuel cell performance.

An alternative solution is to increase the airflow as the atmospheric pressure reduces, compensating for the oxygen mass lowering due to the partial pressure through the increasing flow. Indeed, equation 10 can reformulated as:

$$\dot{n}_i = \gamma_i p_i \dot{V}_i \tag{26}$$

Therefore, product $p_i\dot{V}_i$ should be maintained to maintain a constant mass flow, $\dot{n}_i$. Using equation 13, yields:

$$\dot{n}_i = \gamma_i x_i p_{atm} \dot{V}_i \tag{27}$$

Because γ_i and x_i are constant, the product $p_{atm}\dot{V}_i$ should remain.

Equation 27 applies to oxygen and hydrogen indistinctively.

3. Engineering Design and Operation of the Control System

From the previous analysis, two solutions arise: regulating hydrogen flow pressure or adapting the airflow to atmospheric pressure variation. Both solutions merge into the same point, maintaining the hydrogen/oxygen molecular flow balance at the fuel cell.

Hydrogen or oxygen flow control has advantages and drawbacks, as shown in Table 1.

Table 1 Advantages and drawbacks of hydrogen and oxygen mass flow control.

Hydrogen flow control		Oxygen flow control	
Advantages	Drawbacks	Advantages	Drawbacks
• More Accurate • Avoids compressor for wasted hydrogen compression • Reduces hydrogen flow energy consumption	• Requires a pressure regulator (more complex design) • Higher cost	• Less complex design and cheaper • Higher heat removal	• Less accurate • Subject to sudden meteorological changes • Requires an oxygen flow control unit

The analysis of Table 1 shows that there is no optimum solution since every option has advantages and drawbacks. The hydrogen flow control system regulates the fuel flow (hydrogen) with more accuracy due to the regulator's higher precision. On the other hand, since there is no wasted hydrogen, the system does not require compressing it, reducing the energy used for hydrogen recirculation back to the storage tank. The system, however, needs a regulator, which is complex and expensive.

The oxygen flow control system has a less complex design, which reduces the cost; nevertheless, the flow regulation control is less accurate, and the oxygen flow depends on meteorological changes, which may reduce the system's performance.

The hydrogen flow control requires a pressure regulator similar to those used in scuba diving, which balances outer water pressure by increasing the inlet airflow.

The hydrogen flow regulator (Figure 2) operates this way:

1. Air enters the regulator case through the air inlets and fills the upper section above the membrane.
2. The membrane moves downwards due to the atmospheric air pressure.
3. The membrane disk pushes down the lever. It forces the valve control mechanism to move to the right, pulling the opening valve and letting the hydrogen flow circulate from the hydrogen inlet hose to the chamber.
4. Hydrogen continues flowing until the pressure in the hydrogen chamber equalizes air pressure.
5. The lever moves upwards as long as hydrogen continues pushing up the membrane disk; the process stops when the pressure equalizes, and the membrane returns to its original position.
6. Hydrogen in the hydrogen chamber circulates to the hydrogen outlet hose due to the pressure difference between the hydrogen chamber and the fuel cell.

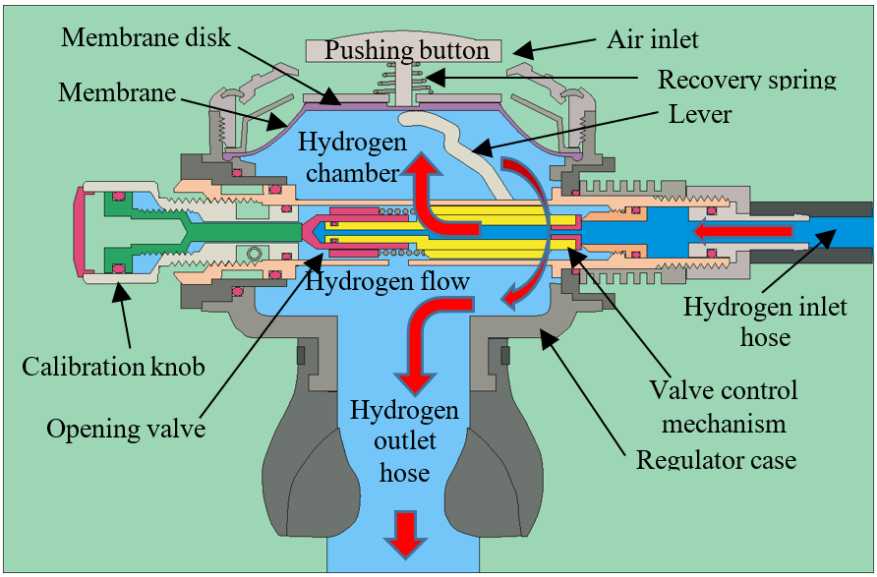

Figure 2 Cross-section of the hydrogen flow pressure regulator [32].

If the fuel cell requires extra hydrogen flow, the system can push down the pushing button, repeating steps 2 and 3 of the above-described process, letting the hydrogen flow to the chamber. After releasing the manual pressure on the pushing button, the recovery spring returns the valve control mechanism to its original position, closing the opening valve and blocking the hydrogen flow.

The regulator equips a calibration knob to regulate hydrogen pressure to the appropriate value for optimum fuel cell performance.

The oxygen flow control system operates under the basis of an opening valve regulated by a control mechanism, which is activated by the current generated by a piezoelectric device submitted to the atmospheric pressure (Figure 3).

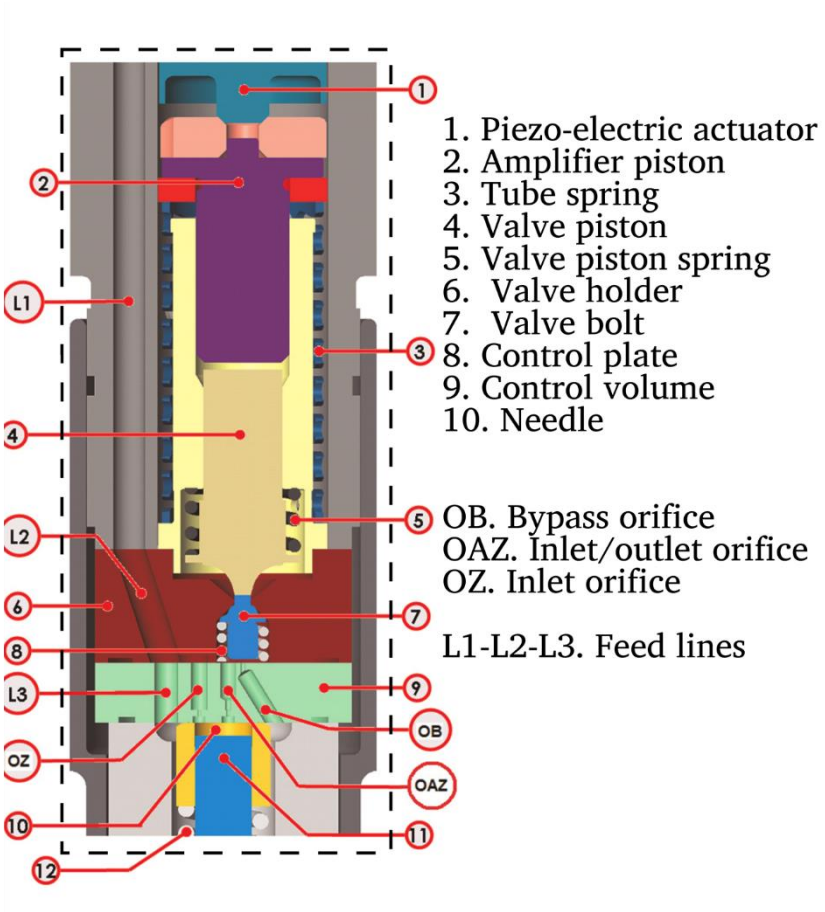

Figure 3 Schematic view of a piezoelectric controlled opening valve [33].

The hydrogen flow regulator operates this way:

1. Air exerts pressure on the piezoelectric actuator, transmitting the pressure to the amplifier piston, which displaces the valve piston downwards, closing or opening the valve and reducing or increasing the airflow depending on operating conditions.
2. The air flows through the valve passage, enters the control volume, and circulates to the outlet hose.

4. Power and Driving Range

Oxygen partial pressure changes derive from atmospheric pressure variation, which happens with meteorological or altitude variation. The first situation is out of human control, but the second is significant, especially in journeys where the road goes through abrupt orographic zones.

In cases where the altitude variation is permanent, the solution to a change in the atmospheric pressure, thus in the oxygen partial pressure, is to modify the hydrogen flow pressure to match the oxygen partial pressure, maintaining the balance in the oxidation-reduction process. If the altitude variation is not permanent, like on roads through rough terrain, the fuel cell system loses power if the hydrogen flow pressure remains unchanged. For example, we consider a typical road in mountainous regions, like the one shown in Figure 4.

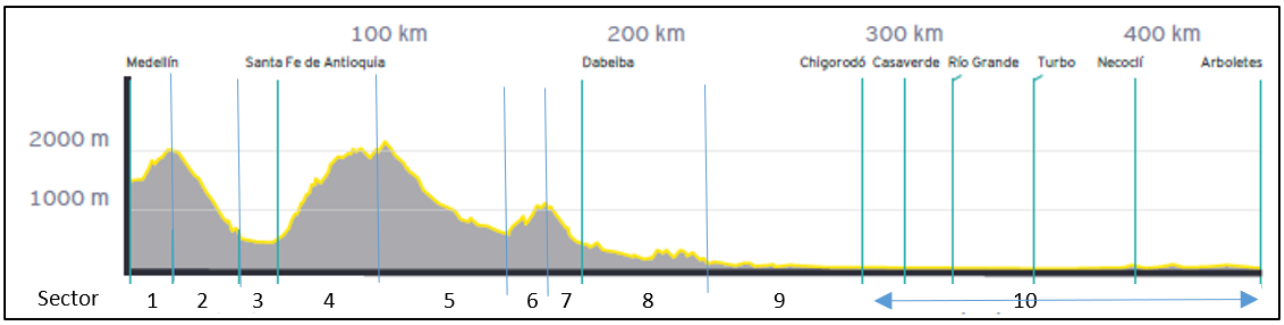

Figure 4 Road orographic profile: Medellín-Arboletes (Colombia) [34].

It can be noticed in Figure 4 that the road suffers from continuous altitude variation in sectors 1, 2, 4, 5, 6, 7, and 8, maintaining constant altitude in the other sectors within acceptable limits.

Since the road profile follows a linear variation when the altitude changes, it may be considered that atmospheric pressure also changes linearly; therefore, the average altitude in every sector is taken to evaluate the output power change. To do so, we determine every sector's initial and final altitude (Table 2).

Table 2 Altitude (m) and distance (km) of the road sectors.

Sector	1	2	3	4	5	6	7	8	9	10
Initial	1351	1824	551	440	1863	545	958	386	231	0
Final	1824	551	440	1863	545	958	386	231	0	0
Distance	16	28	16	40	55	15	15	38	33	145

Applying equation 23, the power factor for every sector results (Table 3):

Table 3 Power factor and power loss for the road sectors.

Sector	1	2	3	4	5	6	7	8	9	10
Av. alt. (m)	1587.5	1187.5	495.5	1151.5	1204.0	751.5	672.0	308.5	115.5	0
F_P	0.841	0.881	0.950	0.885	0.880	0.925	0.933	0.969	0.988	1.0
P_L (%)	15.9	11.9	5.0	11.5	12.0	7.5	6.7	3.1	1.2	0

Notice that power loss is significant in some road sectors, with values near 16% at the maximum point and an average value of 7.5%. The power loss distribution, however, is irregular, depending on the selected sector; therefore, the influence on hydrogen consumption is variable.

Considering a fuel cell without a hydrogen or oxygen flow control system, equipping a vehicle traveling on a mountainous road like the one shown in Figure 4, the power loss influences the energy consumption; the situation leads to a higher hydrogen consumption and a driving range reduction.

We can determine the energy and hydrogen consumption increase and the reduction in the driving range by using data from Table 3.

Assuming the hydrogen mass in the vehicle storage tank is enough to complete the journey at specific driving conditions:

$$\xi_T = \sum_{i=1}^{10} \xi_i = \sum_{i=1}^{10} P_{t,i} t_i \tag{28}$$

ξ represents the energy consumption, P_t is the power, and t is the running time. Sub-indexes T and i account for the whole journey and a single sector.

Power supply comes from the hydrogen consumption according to the hydrogen-specific power, L_{H_2}:

$$P_t = m_{H_2} L_{H_2} \tag{29}$$

The hydrogen specific power is 142 MJ/kg [35].

The hydrogen consumption for a specific route sector is:

$$m_{H_2}|_i = \frac{\xi_i}{L_{H_2}} = \frac{P_{t,i} t_i}{L_{H_2}} \tag{30}$$

Since the sector traveling time must remain constant, regardless of the operating conditions of the fuel cell, the hydrogen consumption rate depends on the power requirement, as in:

$$\dot{m}_{H_2}|_i = \frac{P_{t,i}}{L_{H_2}} \tag{31}$$

From this, we have:

$$P_{t,i} = \dot{m}_{H_2,i} L_{H_2} \tag{32}$$

Combining equations 30 and 32:

$$\xi_i = \dot{m}_{H_2,i} L_{H_2} t_i \tag{33}$$

Now, considering that the power supply to achieve the required energy for travelling a road sector comprises two terms, the current power supply, and the power loss, yields:

$$\xi_i = \left(\dot{m}_{H_2}|_o + \Delta\dot{m}_{H_2}\right) L_{H_2} t_i \tag{34}$$

The term $\Delta\dot{m}_{H_2}$ is given by:

$$\Delta\dot{m}_{H_2} = \frac{\Delta P_{t,i}}{L_{H_2}} \tag{35}$$

$\Delta P_{t,i}$ corresponds to the power loss due to the non-use of the hydrogen, or oxygen, flow control system.

Applying data from Table 3, using Equation 25, and the hydrogen-specific power value, we obtain the extra hydrogen mass flow (Table 4):

Table 4 Extra hydrogen mass flow for the road sectors per unit power.

Sector	1	2	3	4	5	6	7	8	9	10
$\Delta\dot{m}_{H_2}$ (g/s)	4.031	3.017	1.268	2.916	3.042	1.901	1.699	0.786	0.030	0

Since the required power depends on dynamic driving conditions and vehicle characteristics, we normalize the additional hydrogen mass flow per unit power; therefore, to determine the absolute value of extra hydrogen mass flow, the user only has to multiply the value from Table 4 by the required power in every road sector.

5. Simulation

From the classical dynamic expression for the power:

$$P_t = Fv \tag{36}$$

where *F* is the global dynamic force on the vehicle, and *v* is the vehicle's average speed, resulting:

$$\Delta\dot{m}_{H_2} = (1 - F_P)\frac{F_i v_i}{L_{H_2}} \tag{37}$$

The global dynamic force, F_T, depends on vehicle mass (m_{EV}), speed (v), acceleration (a), drag (κ) and rolling (μ) coefficients, and road slope (α). From the dynamic laws:

$$F_T = (m_{EV}a + \kappa v^2 + \mu m_{EV}g + m_{EV}g\sin\alpha) \tag{38}$$

Because combining all dynamic parameters is too high, standard values are used to determine the global dynamic force. Table 5 shows the selected values for the dynamic parameters.

Table 5 Dynamic values for the simulation.

Mass (kg)	Speed (km/h)	Acceleration (m/s^2)	Slope (°)
1650	40	0	0
3500	60	1.5	1
10000	80	2.5	3
40000	100	3.5	5

Using all possible combinations of selected values for the dynamic parameters to the road profile in Figure 4 may result in inconsistent dynamic situations; therefore, we reduce the combinations to those compatible with current driving conditions, yielding the following cases (Table 6). All vehicle mass options are feasible, representing from top to bottom: light-duty, van, small truck, and heavy lorry.

Table 6 Compatible dynamic parameters combination with driving conditions.

Speed →	40 km/h		60 km/h			80 km/h		
	Slope (%)		Slope (%)			Slope (%)		
Acceleration (m/s^2) ↓	2	5	0	2	5	0	2	5
0	C1A	C1B	C2A	C2B	C2C	C3A	C3B	C3C
1.75	C4A		C5A	C5B				
2.5			C6					
3.5			C7					

The blank space in Table 6 corresponds to a non-applicable case.

The next development step in the simulation is determining which case corresponds to every road sector; if a specific case cannot describe the whole industry, two or more cases are assigned.

Analyzing the different sectors in Figure 4, the following road sector configuration can be obtained (Figure 5).

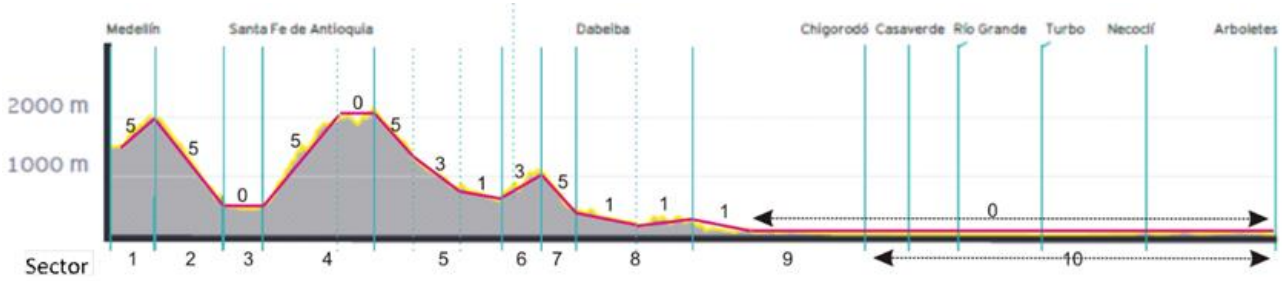

Figure 5 Road slope (%) by road sector.

Combining the results from Table 6 with the road orographic profile in Figure 5, we obtain the applicable cases for every road sector (Figure 6).

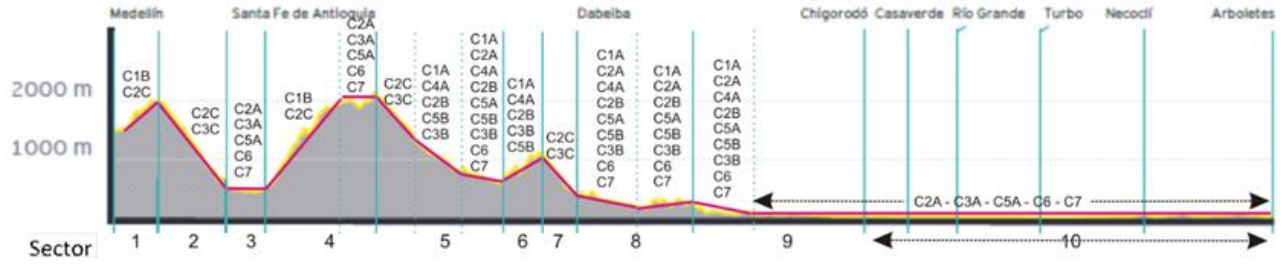

Figure 6 Application cases by road sector.

Applying data from Table 5 and Table 6 to equation 36, and considering a drag and rolling coefficient of 0.04 and 0.015, it results (Table 7 and Table 8).

Table 7 Global dynamic force (N).

Mass	C1A	C1B	C2A	C2B	C2C	C3A	C3B
1650	813	1659	255	820	1666	265	830
3500	1719	3513	527	1726	3520	537	1735
10000	4901	10027	1484	4907	10034	1493	4917
40000	19586	40091	5898	19593	40098	5908	19602
	C3C	C4A	C5A	C5B	C6	C7	
1650	1675	3701	3143	3708	4380	6030	
3500	3529	7844	6652	7851	9277	12777	
10000	10043	22401	18984	22407	26484	36484	
40000	40108	89586	75898	89593	105898	145898	

Table 8 Power (kW).

Mass	C1A	C1B	C2A	C2B	C2C	C3A	C3B
1650	9.0	18.4	4.3	13.7	27.8	5.9	18.4
3500	19.1	39.0	8.8	28.8	58.7	11.9	38.6
10000	54.5	111.4	24.7	81.8	167.2	33.2	109.3
40000	217.6	445.5	98.3	326.5	668.3	131.3	435.6
	C3C	C4A	C5A	C5B	C6	C7	
1650	37.2	41.1	52.4	61.8	73.0	100.5	
3500	78.4	87.2	110.9	130.8	154.6	213.0	
10000	223.2	248.9	316.4	373.5	441.4	608.1	
40000	891.3	995.4	1265.0	1493.2	1765.0	2431.6	

Considering that the driving conditions are not applicable if the required power exceeds a threshold, which in our case is 2500 kW. This threshold corresponds to a technical limitation in manufacturing economically profitable electric motors. Therefore, cases with required power above the threshold are not considered for the global dynamic calculation.

Now, retrieving data from Table 4 and Table 8, applying Equation 28, and considering the driving conditions and traveling time for every sub-sector, we can obtain the additional hydrogen mass consumption if the system does not operate with hydrogen or oxygen flow control. The traveling time is determined considering a constant vehicle speed.

Since some sectors include variable-slope subsectors, data can be written in various character types to distinguish one slope from another. Table 9 and Table 10 show the simulation results for every case and sector.

The character type is as follows:

- Normal type: road slope 0%.
- Italic type: road slope 1%.
- Bold italic type: road slope 3%.
- Bold type: road slope 5%.

Table 9 Additional hydrogen consumption (g).

		Sector									
EV mass (kg)	*Case*	*1*	*2*	*3*	*4*	*5*	*6*	*7*	*8*	*9*	*10*
	C1A	---	---	---	---	***81.3***	***25.4***	---	*74.3*	*109.9*	*0*
	C1B	***27.9***	---	---	***34.4***	---	---	---	---	---	*0*
	C2A	---	---	*18.8*	***53.6***	*61.1*	---	---	*55.9*	*82.6*	*0*
	C2B	---	---	---	---	***81.9***	***25.6***	---	*74.9*	*110.8*	*0*
	C2C	***74.3***	***2.1***	---	***3.4***	***3.9***	---	***1.1***	---	---	*0*
	C3A	---	---	*1.3*	***3.6***	---	---	---	---	---	*0*
1650	*C3B*	---	---	---	---	***36.3***	***11.3***	---	*33.2*	*49.1*	*0*
	C3C	---	***44.3***	---	---	***50.6***	---	***13.7***	---	---	*0*
	C4A	---	---	---	---	***139.4***	***43.5***	---	*127.5*	*188.5*	*0*
	C5A	---	---	*11.2*	***34.4***	*39.2*	---	---	*35.8*	*53.0*	*0*
	C5B	---	---	---	---	***59.1***	***18.4***	---	*54.0*	*79.8*	*0*
	C6	---	---	*2.8*	***7.9***	*9.0*	---	---	*8.3*	*12.2*	*0*
	C7	---	---	*3.9*	***11.0***	*12.5*	---	---	*11.4*	*16.9*	*0*

The standard hydrogen consumption for a light-duty vehicle of 1650 kg with a standard energy consumption of 165 Wh/km is (Table 10):

Table 10 Standard hydrogen consumption (g).

		Sector									
EV mass (kg)	Case	1	2	3	4	5	6	7	8	9	10
	C1A	---	---	---	---	***488.2***	***152.3***	---	*446.3*	660.0	1572.9
	C1B	**167.3**	---	---	**642.0**	---	---	---	---	---	1572.9
	C2A	---	---	225.4	***642.0***	*732.2*	---	---	*669.5*	990.0	2359.3
	C2B	---	---	---	---	***732.2***	***228.5***	---	*669.5*	990.0	2359.3
	C2C	**251.0**	**21.2**	---	**642.0**	**732.2**	---	**197.9**	---	---	2359.3
	C3A	---	---	300.6	***856.0***	---	---	---	---	---	3145.8
1650	C3B	---	---	---	---	***976.3***	***304.6***	---	*892.6*	1320.0	3145.8
	C3C	---	**395.6**	---	---	**976.3**	---	**263.9**	---	---	3145.8
	C4A	---	---	---	---	***488.2***	***152.3***	---	*446.3*	660.0	1572.9
	C5A	---	---	300.6	***642.0***	*732.2*	---	---	*669.5*	990.0	2359.3
	C5B	---	---	---	---	***732.2***	***228.5***	---	*669.5*	990.0	2359.3
	C6	---	---	225.4	***642.0***	*732.2*	---	---	*669.5*	990.0	2359.3
	C7	---	---	225.4	***642.0***	*732.2*	---	---	*669.5*	990.0	2359.3

Data from Table 9 shows that sector 10, corresponding to zero road slope, does not represent a significant variation in the hydrogen mass flow; therefore, the hydrogen and oxygen supply pressure to the fuel cell should be adjusted for the flat terrain, as it does not introduce, or barely does, changes in the fuel cell performance.

The additional hydrogen consumption for an electric vehicle's mass of 3500, 10000, and 40000 kilograms can be obtained by simply multiplying the values shown in Table 9 by the mass ratio.

Simulating every case to verify the above statement, obtaining the following results (Table 11):

Table 11 Additional hydrogen mass ratio for variable vehicle mass.

Vehicle mass (kg)	3500	10000	40000
Vehicle mass ratio	2.121	6.061	24.242
H_2 mass flow ratio	2.103	5.976	23.855
Deviation (%)	0.9	1.4	1.6

Notice the low deviation between the vehicle mass ratio and the hydrogen mass ratio, below 1.6% in the three cases, validating the calculation method for the additional hydrogen mass based on data from Table 9 and the vehicle mass ratio.

Now, comparing data from Table 9 and Table 10, the hydrogen wasting percentage for every case is determined (Table 12).

Table 12 Hydrogen wasting percentage.

		Sector										
EV mass (kg)	Case	1	2	3	4	5	6	7	8	9	10	average
	C1A	---	---	---	---	***16.7***	***16.7***	---	*16.6*	16.7	0	16.7
	C1B	**16.7**	---	---	**5.4**	---	---	---	---	---	0	11.1
	C2A	---	---	8.3	***8.3***	*8.3*	---	---	*8.3*	8.3	0	8.3
	C2B	---	---	---	---	***11.2***	***11.2***	---	*11.2*	11.2	0	11.2
	C2C	**29.6**	**9.9**	---	**0.5**	**0.5**	---	**0.6**	---	---	0	8.2
	C3A	---	---	0.4	***0.4***	---	---	---	---	---	0	0.4
1650	C3B	---	---	---	---	***3.7***	***3.7***	---	*3.7*	3.7	0	3.7
	C3C	---	**11.2**	---	---	**5.2**	---	**5.2**	---	---	0	7.2
	C4A	---	---	---	---	***28.6***	***28.6***	---	*28.6*	28.6	0	28.6
	C5A	---	---	3.7	***5.4***	*5.4*	---	---	*5.3*	5.4	0	5.0
	C5B	---	---	---	---	***8.1***	***8.1***	---	*8.1*	8.1	0	8.1
	C6	---	---	1.2	***1.2***	*1.2*	---	---	*1.2*	1.2	0	1.2
	C7	---	---	1.7	***1.7***	*1.7*	---	---	*1.7*	1.7	0	1.7

6. Data Analysis

Analyzing data from Table 12, the following results apply:

Sector 1 shows the highest hydrogen wasting mass for the two analyzed cases. The extra hydrogen mass required depends on vehicle speed: 16.7% for 40 km/h and 29.6% for 60 km/h. The hydrogen wasting mass to vehicle speed ratio increases with this last parameter because of a higher drag force.

Sector 2 shows a relatively moderate wasting mass for the two analyzed cases, with no significant dependence on vehicle speed.

Sector 3, which corresponds to relatively flat terrain, shows low hydrogen wasting percentage except for low vehicle speed, zero road slope, and no acceleration, which looks incoherent. Nevertheless, the same driving conditions applied to other sectors, 4, 5, 8, and 9, with different orographic characteristics, result in identical hydrogen wasting percentages. We attribute this apparent behavior abnormality to poorer fuel cell performance.

The hydrogen wasting percentage for sector 4 is variable. The fuel cell performance improves as the vehicle speed, acceleration, and road slope increase. These results indicate that the fuel cell performance is poorer at low power demand.

The high variability in hydrogen wasting percentage for sector 5 is due to the large number of analyzed cases, comprising a wide range of driving conditions. It calls attention to case C4A, which corresponds to low vehicle speed, acceleration, and road slope and shows the highest wasting percentage. This result confirms the statement of a low fuel cell performance for these driving conditions.

Sector 6 shows similar results to Sector 5, confirming the evolution of fuel cell performance for the variable driving conditions statement mentioned before.

When comparing the results from sector 7 to those from sector 2, both corresponding to relatively descending roads with a 5% slope, a lower value in the hydrogen wastage percentage can be observed. This suggests that the fuel cell performs better as the altitude decreases.

Sectors 8 and 9 show identical results to Sectors 5 and 6, confirming the statements about the fuel cell performance.

In sector 10, no hydrogen is wasted because the fuel cell operates at standard reference conditions.

Analyzing the different cases, which correspond to variable driving conditions, we should notice that the fuel cell performance is regular, independent of the road sector. The only disagreement corresponds to sector 1, where the higher hydrogen wasting percentage is attributed to a poorer fuel cell performance because of the starting, with the operating temperature being a key factor for the system behavior.

7. Driving Range

The increase in hydrogen supply to compensate for the performance lowering means a reduction in the driving range. Operating with a specific hydrogen tank containing pressurized gas, the available mass is given by:

$$m_{H_2} = V_{tk}\rho_{H_2} = p_{tk}V_{tk}\rho^o_{H_2} \tag{39}$$

V_{tk} and p_{tk} are the tank volume and pressure, and ρ_{H_2} is the hydrogen density, with the super-index *o* indicating standard conditions at atmospheric pressure.

Considering a standard consumption rate, $\dot{\zeta}^o_{H_2}$, in kg/km, the driving range is:

$$DR^o = \frac{m_{H_2}}{\dot{\zeta}^o_{H_2}} = \frac{p_{tk}V_{tk}\rho^o_{H_2}}{\dot{\zeta}^o_{H_2}} \tag{40}$$

If the consumption rate increases due to a poorer fuel cell performance, the driving range modifies according to:

$$DR = \frac{p_{tk} V_{tk} \rho^o_{H_2}}{\dot{\zeta}_{H_2}} = \frac{p_{tk} V_{tk} \rho^o_{H_2}}{F_{cr} \dot{\zeta}^o_{H_2}} \tag{41}$$

The coefficient F_{cr} is the consumption rate factor, which includes the extra hydrogen supply to compensate for the performance loss.

Expressing F_{cr} in terms of the hydrogen wasting percentage:

$$DR = \frac{p_{tk} V_{tk} \rho^o_{H_2}}{\left(1 + \frac{\Delta m_{H_2}}{m^o_{H_2}}\right) \dot{\zeta}^o_{H_2}} \tag{42}$$

Δm_{H_2} represents the hydrogen wasting mass, and $m^o{}_{H2}$ is the standard fuel cell hydrogen consumption taken as the reference value. The term between parentheses is the hydrogen wasting percentage.

Analyzing equation 42, the reader can notice that the driving range reduces as the hydrogen wasting percentage increases.

Since the driving conditions evolve along the route, it is difficult to evaluate the hydrogen wasting percentage for constant operating conditions; therefore, we decided to operate with two different configurations: first, averaging all cases, and second, considering the driving conditions closest to the conventional driving mode, which are, 40 km/h in uphill road with no acceleration, 60 km/h in downhill road with no acceleration either, and 80 km/h in flat terrain with intermediate acceleration value.

Applying these driving conditions, the selected cases are (Table 13):

Table 13 Selected cases for every road sector for hydrogen wasting percentage evaluation in the closest driving conditions to standard ones.

Sector	1	2	3	4	5	6	7	8	9
Case	C1B	C2C	C5A	C1B	C2B	C5B	C3C	C3B	C3B

a) Global average value

Averaging values from Table 12, and applying equation 40, yields:

$$DR = \frac{p_{tk} V_{tk} \rho^o_{H_2}}{1.0846 \dot{\zeta}_{H_2}} = 0.922 DR^o \tag{43}$$

b) Near standard driving conditions

Repeating the process for the second assumption:

$$DR = \frac{p_{tk} V_{tk} \rho^o_{H_2}}{1.0751 \dot{\zeta}^o_{H_2}} = 0.930 DR^o \tag{44}$$

The reader should notice the close agreement between the global average and the near-standard driving conditions case, with a difference of 0.9% in the consumption correction factor. Therefore,

the global average can be used as the reference value since it represents all the possible driving conditions.

The driving range analysis shows a reduction of about 7% to 8% if the electric vehicle operates with a standard fuel cell not equipped with a hydrogen/oxygen flow control unit.

8. Fuel Cell Application

Although the proposed methodology applies to PEMFC, the process is valid for other fuel cells provided they work with atmospheric oxygen like the Direct Methanol Fuel Cell (DMFC), which operates with a mixture of water and liquid methanol supply to the anode and atmospheric air supply to the cathode, according to the overall chemical reaction:

$$CH_3OH + \frac{3}{2}O_2 \rightarrow CO_2 + 2H_2O \tag{45}$$

And anode and cathode reactions:

$$\begin{gathered} CH_3OH + H_2O \rightarrow CO_2 + 6H^+ + 6e^-(anode) \\ 6H^+ + 6e^- + (3/2)O_2 \rightarrow 3H_2O(cathode) \end{gathered} \tag{46}$$

Alkaline Fuel Cell (AFC) is another case in which the proposed methodology applies since it operates with an atmospheric oxygen supply. As in the DMFC case, the anode and cathode reactions are:

$$\begin{gathered} H_2 + 2OH^- \rightarrow 2H_2O + 2e^-(anode) \\ (1/2)O_2 + H_2O + 4e^- \rightarrow 2OH^-(cathode) \end{gathered} \tag{47}$$

For the overall reaction:

$$H_2 + (1/2)O_2 \rightarrow H_2O \tag{48}$$

The Solid Oxide Fuel Cell (SOFC) is a third additional case where the proposed method applies since it uses atmospheric oxygen for the cathodic chemical reaction to produce oxygen ions according to:

$$\begin{gathered} (1/2)O_2 + 2e^- \rightarrow O^*(cathode) \\ H_2 + O^* \rightarrow H_2O + 2e^-(anode) \end{gathered} \tag{49}$$

For the overall reaction:

$$H_2 + (1/2)O_2 \rightarrow H_2O \tag{50}$$

As we see, the fuel mentioned above cells operate with an atmospheric oxygen supply, allowing the proposed methodology to be applied.

9. Conclusions

The principal contribution of this work to the state of the art is the system operation with a hydrogen pressure regulator and an optional oxygen pressure regulator to improve the system

operation efficiency, adjusting the hydrogen and oxygen mass supply to the working conditions. The methodology and materials used for this purpose are clearly described in this paper, helping designers and manufacturers to implement the proposed solution.

Electric vehicles powered by a fuel cell show variable behavior when operating on roads with continuous altitude variation. The changes in atmospheric pressure influence the fuel cell performance due to an oxygen partial pressure variation, which dysregulates the standard operational conditions of the fuel cell. Fuel cell performance lowering depends on driving and road conditions, with specific reduction at low power demand. Fuel cell requires an extra hydrogen mass supply to compensate for the performance reduction; the supply value depends on driving conditions, moving from a minimum of 0.4% for flat terrain and highest vehicle speed with no acceleration to a maximum of 29.6% for uphill road with maximum slope and intermediate vehicle speed with no acceleration. If we average all driving and road conditions, the hydrogen wasting percentage is 8.46%.

The hydrogen wasting shows high variability in percentage value, depending on driving conditions; nevertheless, testing the global average value for all cases and driving conditions and the near standard driving mode matches with 99% accuracy. Therefore, we can use the global average value as a reference. It also reduces the driving range due to the extra fuel supply to compensate for the fuel performance loss; applying the correction factor for the hydrogen mass supply, which is the same as the global average hydrogen wasting percentage value, the driving range is reduced by 7.8%.

This study is relevant for the design of fuel cell units powering electric vehicles that operate in regions with abrupt orographic profiles since the implementation of an accurate control system like the one described in this work improves fuel cell performance, extends the driving range, and saves energy, representing a critical advance in future fuel cell electric vehicle development.

Author Contributions

The author did all the research work of this study.

Competing Interests

The author has declared that no competing interests exist.

References

1. Van der Zwaan B, Keppo I, Johnsson F. How to decarbonize the transport sector? Energy Policy. 2013; 61: 562-573.
2. De Abreu VH, Da Costa MG, Da Costa VX, De Assis TF, Santos AS, D'Agosto MD. The role of the circular economy in road transport to mitigate climate change and reduce resource depletion. Sustainability. 2022; 14: 8951.
3. La Notte A, Tonin S, Lucaroni G. Assessing direct and indirect emissions of greenhouse gases in road transportation, taking into account the role of uncertainty in the emissions inventory. Environ Impact Assess Rev. 2018; 69: 82-93.
4. Newman P, Kenworthy J. Evaluating the transport sector's contribution to greenhouse gas emissions and energy consumption. In: Technologies for climate change mitigation-transport

sector. Copenhagen, Denmark: UNEP Risoe Centre on Energy, Climate and Sustainable; 2011. pp. 7-23.
5. Block F. Innovation and the invisible hand of government. State of innovation. London, UK: Routledge; 2015.
6. Hoffmann P. Tomorrow's energy, revised and expanded edition: Hydrogen, fuel cells, and the prospects for a cleaner planet. Cambridge, MA: MIT Press; 2012.
7. Goonan TG. Lithium use in batteries. Reston, VA: US Geological Survey; 2012.
8. Zeng X, Li M, Abd El-Hady D, Alshitari W, Al-Bogami AS, Lu J, et al. Commercialization of lithium battery technologies for electric vehicles. Adv Energy Mater. 2019; 9: 1900161.
9. Speirs J, Contestabile M, Houari Y, Gross R. The future of lithium availability for electric vehicle batteries. Renew Sustain Energy Rev. 2014; 35: 183-193.
10. Wanger TC. The lithium future-resources, recycling, and the environment. Conserv Lett. 2011; 4: 202-206.
11. Narins TP. The battery business: Lithium availability and the growth of the global electric car industry. Extr Ind Soc. 2017; 4: 321-328.
12. Kushnir D, Sandén BA. The time dimension and lithium resource constraints for electric vehicles. Resour Policy. 2012; 37: 93-103.
13. Reuter B, Riedl J, Hamacher T, Lienkamp M, Bradshaw AM. Future resource availability for the production of lithium-ion vehicle batteries. CoFAT; 2014. Available from: https://mediatum.ub.tum.de/doc/1226680/document.pdf.
14. Contestabile M, Offer GJ, Slade R, Jaeger F, Thoennes M. Battery electric vehicles, hydrogen fuel cells and biofuels. Which will be the winner? Energy Environ Sci. 2011; 4: 3754-3772.
15. Wanitschke A, Hoffmann S. Are battery electric vehicles the future? An uncertainty comparison with hydrogen and combustion engines. Environ Innov Soc Transit. 2020; 35: 509-523.
16. Lubitz W, Tumas W. Hydrogen: An overview. Chem Rev. 2007; 107: 3900-3903.
17. Rigden JS. Hydrogen: The essential element. Cambridge, MA: Harvard University Press; 2003.
18. Abdin Z, Zafaranloo A, Rafiee A, Mérida W, Lipiński W, Khalilpour KR. Hydrogen as an energy vector. Renew Sustain Energy Rev. 2020; 120: 109620.
19. Singh S, Jain S, Venkateswaran PS, Tiwari AK, Nouni MR, Pandey JK, et al. Hydrogen: A sustainable fuel for future of the transport sector. Renew Sustain Energy Rev. 2015; 51: 623-633.
20. Ahmed A, Al-Amin AQ, Ambrose AF, Saidur R. Hydrogen fuel and transport system: A sustainable and environmental future. Int J Hydrogen Energy. 2016; 41: 1369-1380.
21. Salvi BL, Subramanian KA. Sustainable development of road transportation sector using hydrogen energy system. Renew Sustain Energy Rev. 2015; 51: 1132-1155.
22. Pramuanjaroenkij A, Kakaç S. The fuel cell electric vehicles: The highlight review. Int J Hydrogen Energy. 2023; 48: 9401-9425.
23. Barbir F. PEM fuel cells: Theory and practice. Cambridge, MA: Academic Press; 2012.
24. Srinivasan S. Fuel cells: From fundamentals to applications. Berlin, Germany: Springer Science & Business media; 2006.
25. Naimi Y, Antar A. Hydrogen generation by water electrolysis. Advances in hydrogen generation technologies. Norderstedt, Germany: Books on Demand; 2018.

26. Tang D, Tan GL, Li GW, Liang JG, Ahmad SM, Bahadur A, et al. State-of-the-art hydrogen generation techniques and storage methods: A critical review. J Energy Storage. 2023; 64: 107196.
27. Zhang JZ, Li J, Li Y, Zhao Y. Hydrogen generation, storage and utilization. Hoboken, NJ: John Wiley & Sons; 2014.
28. Rasul MG, Hazrat MA, Sattar MA, Jahirul MI, Shearer MJ. The future of hydrogen: Challenges on production, storage and applications. Energy Convers Manage. 2022; 272: 116326.
29. Abdalla AM, Hossain S, Nisfindy OB, Azad AT, Dawood M, Azad AK. Hydrogen production, storage, transportation and key challenges with applications: A review. Energy Convers Manage. 2018; 165: 602-627.
30. Climate Change Trust. All about fuel cells [Internet]. Climate Change Trust; 2024. Available from: https://www.fuelcellscars.com/Fuel_Cells_All_About_How_Do_They_Work.htm.
31. Haseli Y. Maximum conversion efficiency of hydrogen fuel cells. Int J Hydrog Energy. 2018; 43: 9015-9021.
32. Wikimedia Commons. File: Scuba regulator 2nd stage animation.gif [Internet]. Wikimedia Commons; 2024. Available from: https://commons.wikimedia.org/wiki/File:Scuba_regulator_2nd_stage_animation.gif.
33. Salvador FJ, Plazas AH, Gimeno J, Carreres M. Complete modelling of a piezo actuator last-generation injector for diesel injection systems. Int J Engine Res. 2014; 15: 3-19.
34. EPM. Homepage [Internet]. Medellín, Colombia: EPM; 2025. Available from: https://www.epm.com.co/.
35. International Renewable Energy Agency. Hydrogen: Overview [Internet]. Masdar City, United Arab Emirates: International Renewable Energy Agency; 2024. Available from: https://www.irena.org/Energy-Transition/Technology/Hydrogen.